TILTROTOR CONTROL ROBUSTNESS ASSESSMENT TO MODEL UNCERTAINTIES IN HOVER AND NEAR HOVER GROUND EFFECT CONDITIONS

Fabio Riccardi
Flight Control Laws Specialist
Leonardo Helicopters S.p.A.
Cascina Costa di Samarate (VA)
Italy

Luca Viganò
NGCTR-TD Flight Control Laws
Chief Project
Leonardo Helicopters S.p.A.
Cascina Costa di Samarate (VA)
Italy

Francesco Marzagalli
Flight Mechanics Specialist
Leonardo Helicopters S.p.A.
Cascina Costa di Samarate (VA)
Italy

Abstract

The paper discusses the developed methodologies for assessing the dynamic stability robustness of tiltrotor aircraft augmented by Flight Control System, in presence of modeling uncertainties, specifically investigating the Hover/near Hover In Ground Effect conditions. The tiltrotor configuration operating in HIGE is characterized by a complex aerodynamic regime, involving important flight dynamics modelling challenges to be tackled and a certain level of model uncertainties, especially when the aerodynamics characterization available is only CFD based (wind tunnel test data not available). This picture is even more demanding considering the Fly-By-Wire nature of tiltrotor vehicles, where the control laws, generally designed and synthetized adopting bare aircraft dynamics model out of ground effect has to guarantee their effectiveness in ground effect as well. The paper specifically addresses, as case study, the Next Generation Civil Tiltrotor Technology Demonstrator (NGCTR-TD). The NGCTR-TD project is developed under the EU Clean Sky 2 program for defining novel technology for future civil tiltrotor platforms. Therefore, to assess the closed-loop dynamic stability of a new Fly-By-Wire rotorcraft for which no experimental flight data exist yet, as part of the flight clearance process, arises a strong need to properly investigate the sources of model uncertainties and verify the control laws robustness to them.

1. INTRODUCTION

As reported by literature works Ref. [1,2], the tiltrotor configuration operating in HIGE is characterized by a complex aerodynamic regime, where interactions between rotors wakes, nacelles, fuselage, wing, and ground (so called “fountain effects”) heavily influence the rotorcraft response. The development of an aeromechanic model able to capture properly the tiltrotor dynamics in this peculiar flight condition is a challenging task. In Ref. [2] it was declared that the adopted level of mathematical model complexity, low enough to be used also for real-time simulations, was unable to predict interactional aerodynamic nature effects, then they were included empirically, fitting experimental data collected in dedicated wind tunnel test campaign on a 0.2 scale powered rotors XV-15 model. Concerning the NGCTR-TD bare aircraft model development in HIGE, the conducted activities were presented in a previous paper Ref. [3], modelling the “fountain effects” through a polynomial fitting as done in Ref. [1,2], but based only on CFD analysis results, without the validation support of a dedicated wind tunnel experimental activity or flight test campaign. The control laws are generally designed and synthetized adopting bare aircraft dynamics model out of ground effect, but has to guarantee their effectiveness in ground effect as well. Indeed the control laws parameters scheduling as a function of the height from ground is generally not deemed necessary for basic control functions, and would require a reliable height above ground measure (such as that provided by a multiple redundant radio altimeter equipment). Moreover, the very first phases of a rotorcraft prototype flight test campaign are typically conducted, for safety reasons, up to a maximum height where the in ground effect is still consistent, in hover/near hover and with the Flight Control System active, as inherently required for a native Fly-By-Wire vehicle like a tiltrotor. It results crucial, taking into consideration these premises, to assess the control laws robustness to both off-design condition like the HIGE and to model uncertainties due to inaccuracies of the input parameters (e.g., aerodynamics data) and by lack of representativeness.

It is worth to remark that for the NGCTR-TD was not adopted an explicit robust control design approach to model uncertainties, such as the H_∞ in Ref. [4] or the μ-synthesis in Ref. [5], just to mention a few, in order to guarantee a-priori the stability robustness to off-nominal HIGE conditions and uncertain models. The robust stability requirements in terms of desired gain and phase margins are enforced in the adopted structured H_∞ optimization design framework of the control laws (see Ref. [6]), together with performance constraints (i.e. loop shaping), but considering only nominal out of ground effect models and without uncertainties. Then, the robustness assessment in HIGE conditions and in presence of uncertainties is performed afterwards.

The traditional approach to parametric model uncertainty robustness analysis, as discussed in Ref. [7], is to perform a Monte Carlo analysis, running a large number of trial cases where the parameters of the model are varied by their known statistics (covariance matrix used to determine a normal distribution), and the stability and performance of the control system are assessed. To perform this process accurately, a large number of random perturbations must be performed, which may be computationally expensive and time consuming, especially when the bare aircraft model has a large number of states. A new, more efficient approach is showed in Ref. [8] to assess the robustness of a tiltrotor control laws to bare aircraft uncertainty. This approach reduces the number of perturbations because instead of perturbing all the stability and control derivatives of the full-order model, perturbations are made only to the reduced order fuselage rigid body derivatives, and instead of the standard Monte Carlo analysis, an unscented transform of the model parameters statistic is employed. Also in the present work is pursued the demand of build a representative database of uncertain models perturbing a reduced number of model parameters (and their permutations), by means of a physics-based selection approach, exploiting Leornado Helicopters experience on flight dynamics modelling. Starting from the NGCTR-TD bare aircraft non-linear model developed in FLIGHTLAB (Ref. [9]), including the specific adds-on to enhance the representativeness in hover/near hover ground effect conditions thoroughly described in Ref. [3], a number of perturbed models were defined, altering selected aeromechanics parameters (in a proper number of combinations) according to the estimated level of their uncertainty from the nominal value. From each perturbed non-linear model (as well as the nominal one), linearization was computed in specific trim conditions, to cover HIGE operations with mast tilt angle set to 90deg (hovering, low speed forward, sideward, backward flight, at different height above ground), obtaining a database of about 8000 bare aircraft rigid body dynamics linear models (e.g. state-space representations).

The assembly of augmented aircraft linear models database, corresponding to the bare aircraft one, was obtained closing the control loop on the linearized Flight Control System, including actuation, sensors, and control laws. For sake of model order reduction, engine and drive-train linearized dynamics were not included in assembling the augmented A/C linear model on all perturbed bare A/C models, considering the generally minor impact on A/C rigid body stability, as recently described in Ref. [10] for NGCTR-TD aircraft in VTOL configuration. Therefore, only for the nominal model the augmented A/C model is assembled by including also linear drive-train and power-plant dynamics, to perform an enhanced robust stability assessment.

The key features of the developed analysis approach are presented hereafter. First, the augmented A/C dynamic stability is assessed on both nominal and perturbed models, for all the considered trim conditions in HIGE, by properly exploiting the Modal Participation Factor (MPF) technique in Ref. [11] to assign the mode shape to each eigenvalue. The assessment was made against the adopted dynamic stability requirements (in terms of modes placement on root-locus): the FAR TR.181. Then, the robust stability assessment is performed, computing the stability margins of the open-loop transfer function considering the control laws designed on HOGE conditions applied to nominal and perturbed HIGE models, evaluating respectively the control robustness respect to off-design trim conditions alone and combined with the model uncertainties. In the present work, it was preferred to adopt the disk-based stability margins method from Ref. [12, 13]: instead of the classical loop-at-time computing approach, it considers a concurrent perturbation on both gain and phase and on all the channels of the control system at the same time. Therefore, it provides a stronger guarantee of closed-loop stability robustness than the canonical definition of gain and phase margins. The adopted gain/phase margin requirements to assess the control robustness are the ones given in SAE-AS-94900 (Ref. [14]).

The actuators model uncertainties were not considered in building up a whole perturbed models database together with the bare A/C uncertainties, considering the following rationale. The initial NGCTR-TD configuration does not encompass swashplate lateral cyclic actuation, hence only prop-rotors collective pitch and longitudinal cyclic actuators are active in the helicopter configuration. The inclusion of all the permutations associated to nominal, upper tolerance and lower tolerance actuation models involves a huge increasing of database dimension (about 10 times), deemed not justified by the expected minor effects on A/C rigid body stability. As a consequence, the impact of actuation performance spread on augmented A/C stability and robustness will be investigated only by combining the worst-case conditions in terms of modes placement and gain/phase margins, found analyzing perturbed models database including bare A/C only uncertainties, with the perturbed actuation models.

2. BARE AIRCRAFT FLIGHT DYNAMICS MODEL AND PERTURBATION APPROACH

The NGCTR-TD aeromechanic model, developed in FLIGHTLAB, represents a trade-off between the physics and phenomenological based approaches. As identified by Ref. [15] physics based models implement relations between cause and effect, inputs and outputs, governed by the laws of physics. Conversely, phenomenological models are based on purely mathematical relationship derived from measurements (such as wind tunnel aerodynamic data). The aeromechanic model implements a suitable combination of these approaches such to assure the required physics representativeness and computational efficiency needed by real-time pilot in-the-loop simulations. The rotorcraft aeromechanic model is composed by the following sub-components:

- Wing & V-tail: Strip theory coupled with Peters-He finite state inflow model, Ref. [16]
- Fuselage & Nacelles: Body frame of reference tabulated data
- Rotors: Blade Element Theory (BET) coupled with Peters-He finite states wake inflow modeling, Ref. [16]

Appropriate characterization of aerodynamic interference between sources of vorticity field and impinged surfaces is achieved by including the most significant sources/receivers interactions, namely:

- Rotors on: wing, tail, nacelles
- Wing on: fuselage, tail

The strategy adopted to accurately capture the specific ground effects of NGCTR-TD in helicopter mode includes phenomenological corrections applied to both rotors and airframe thoroughly described in Ref. [3], briefly resumed hereafter. Three are the main phenomena to be modelled:

- Prop-rotors behavior in ground effect providing diminished thrust when entering in ground effect conditions due to large portions of stalled rotor blades close to the root.
- Rotors wake impingement on tail via ground altering the longitudinal set of forces and moments (i.e. pitch down effect)
- Rotors wake impingement on the fuselage belly and wings via ground altering the aerodynamic lateral forces and moments in presence of roll attitude (i.e. rolling moment which leads the aircraft to further increase the roll attitude)

Concerning ground effect on prop-rotors, it is enforced in FLIGHTLAB model via an additional dependency of the inflow correction parameter with non-dimensional rotors height above ground (h/D), together with the usual dependencies on advance ratio and wake skew angle. The influence of A/C horizontal ground speed was taken into account too, in order to model the wakes wash-out. About the effects of ground on longitudinal axis, the airframe download correction was introduced in the model through properly tuned coefficient to match the CFD prediction of A/C vertical force and pitching moment, through delta forces and moments on each airframe component (i.e. wing, nacelle, tail and fuselage) scheduled with the non-dimensional rotor height and A/C horizontal ground speed for the exponential decay of the download. Finally, the effect of ground on the lateral axis was modeled with a polynomial expression that corrects the A/C rolling moment as function of h/D, roll angle and ground speed, as showed in Ref. [3], properly adjusted to match the CFD data.

Accordingly to the physics-based approach, a family of 52 uncertain (a.k.a. perturbed) NGCTR-TD FLIGHTLAB models was generated, each of them differs from the nominal one by at least one parametric perturbation. The parameters that have been perturbed are discussed hereafter.

- Blade tip loss factor

Nominally fixed at 96%, the effect of 100% and 88% setting were considered.

- Swashplate phase angle

With respect to the nominal value, the effect of ±1 deg on the swashplate phase angle was studied since deemed sufficient to enclose its uncertainties.

- Prop-rotors gimbal spring stiffness of pitch and roll axis hinge

A variability of ±20% respect to nominal values was deemed enough to capture the uncertainties.

- Tip losses capturing model

A different implementation of the tip losses modelling was adopted to evaluate the deviation from the nominal one. The last enforces a fixed truncation of the blade tip effectiveness, while for the perturbed models the blade tip losses are taken into account via a physics-based model (Ref. [20]).

- Wing morphing and aileron airfoil tables

To include the uncertainties related to rotor downwash on wing morphing and aileron modeling, the aerodynamic tables of these surfaces were perturbed by ±10% respect to nominal on the drag coefficient.

- Nacelle aerodynamic loads

Nacelles are a delicate component of tiltrotors modelling, as their aerodynamics interactions are difficult to be captured but drives important effects on A/C dynamics. For this reason, their impact was largely stressed by considering a perturbed model without nacelles (0% of nominal nacelle loads) and with half of their effect (50% of nominal nacelle loads).

- Prop-rotors download on wings

Prop-rotors wake interference on wings is one of the most remarkable peculiarities, and penalties, of tiltrotors. Native FLIGHTLAB predictions are usually deemed not sufficient to capture these effects, thus wing loads are corrected via CFD data. These corrections are affected by uncertainties, so the perturbed models were generated by considering: no CFD corrections or nominal CFD correction ±10%.

- Prop-rotors interference on wings

For the same reasons reported in the previous point, one perturbed model was generated switching off the rotor interference on wings.

- Prop-rotors airfoil table

It was enforced a reasonable deviation range from the nominal linear portion slope of $C_L(\alpha)$, $C_D(\alpha)$, and $C_M(\alpha)$ blade airfoil coefficients. These deviations account for uncertainties coming from a statistic survey. The effect of this perturbations has relevant effects both on A/C trim and stability.

Considered the complexity of tiltrotor HIGE aerodynamic regime and its modelling uncertainties, wide perturbations were considered on the modelling parameters briefly described in the introductory part of this paragraph, as detailed below.

- HIGE prop-rotors thrust correction

The table accounting for the effect of h/D on prop-rotors thrust was perturbed in the range of ±30% respect to nominal, based on engineering judgment of modeling uncertainties.

- HIGE airspeed exponential decay factor on prop-rotors inflow

The model parameter for exponential wash-out of the ground effects on thrust was perturbed by ±50% respect to nominal value.

- Scaling factor on HIGE rolling moment polynomial formulation

The polynomial function introduced to compute the rolling moment due to ground effects is multiplied by a scaling factor in order to match the CFD prediction of rolling moment derivative respect to roll angle. This value was perturbed in a wide range of ±50% respect to nominal.

- HIGE airframe download correction

Scheduling of delta vertical forces and pitching moments on each airframe component with the non-dimensional rotor height was perturbed in the range of ±30% respect to nominal set.

- Airspeed exponential decay factor on HIGE airframe download correction

The parameter modelling the exponential wash-out of the ground effect on airframe download was perturbed by ±50% respect to nominal.

Once the uncertain models family was built accordingly to above discussed perturbation strategy, in order to properly investigate the reduced flight envelope for the initial phase of NGCTR-TD flight test activities, limited to hover/near hover in ground effect operations (mast tilt angle set to 90deg), 156 trim conditions were computed, with the nominal model and each perturbed one, permuting the following parameters:

- From hovering to 20kts, step 5kts
- Sideslip angle: 0deg (forward flight), 90deg (sideward flight), 180deg (backward flight)
- Non-dimensional height from ground h/D: 0.7, 0.9, 1.2, 1.7
- 3 different aircraft mass configurations representing perturbations around the mid gross weight and the mid longitudinal center of gravity position (i.e. aligned with the mast tilt axis), labelled as:
  - WCG1: W mid minus delta W, CG MID with afterward delta
  - WCG2: W mid, CG MID
  - WCG3: W mid plus delta W, CG MID with forward delta

3. CONTROL LAWS DESIGN

The NGCTR-TD FCS Control Laws implement two main operating modes, Normal Mode and Direct Mode, with distinct functions and Handling Qualities characteristics. For the scope of the present investigation, it suffices to say that:

- Direct Mode is the NGCTR-TD selected mode for this analysis, as it is candidate for initial flight campaign phase. In VTOL mode, it provides conventional rate-command / return-to-trim response characteristics with basic auto-stabilization about longitudinal, lateral and directional axis. Thrust and Power Management System logics are fully functional.
- Normal Mode is the most augmented mode for NGCTR-TD. In VTOL mode, it provides rate-command/attitude-hold response type with auto-trim capability about longitudinal, lateral and directional axis. Besides relying on Thrust and Power Management System functions, the heave axis provides also heave damper augmentation.

Since Direct Mode CLAWs do not make use of body attitude measurements, small authority integral or pseudo-integral (yaw rate leaky integrator added to directional axis) commands has been implemented into legacy tiltrotor SCAS (Stability and Command Augmentation System) logics to improve long-term aircraft stability while in HIGE conditions. These terms behave similarly to proportional attitude stabilization loops (further details on integral terms effects on A/C stability are given in Ref. [3]). Due to unreliable or even unavailable air data in Direct Mode operation, and in any case considering the limited airspeed range applicable to HELO VTOL flight envelope, the Direct Mode CLAWs provide basic mast tilt angle gain schedule, i.e. fixed SCAS gains for a given rotors' thrust vectoring angle. It is therefore straightforward that CLAWs synthesis process must be robust against the expected spread of NGCTR-TD HELO VTOL operating conditions. The Direct Mode Control Laws synthesis process is based on following assumptions:

a) Pure HOGE conditions are used for CLAWs design optimization, as HIGE flight dynamics models would lead to overly conservative SCAS design if not causing failure of design optimization process due to poorly stabilizable low frequency rigid body modes.
b) Nominal NGCTR-TD models feeding gain optimization process, because large set of perturbed models would be too numerically demanding for the Control Laws optimization routines.

It's worth noting that HIGE nominal and perturbed models are used for verification purposes once the Direct Mode Control Laws design is completed. Future activities will investigate how integrate worst-case perturbed conditions into Control Laws design, hence keeping computational burden to reasonable levels. The Control Laws design (tuning) optimization process is based on structured H_∞ optimization, and specifically on algorithm presented in Ref. [6]. The general design requirements enforced during the optimization process are resumed in Table 1.

Control Requirement	Remark
Stability Margins (@Actuators)	SISO loop broken on total stick (pedal) command. Disk margins requirement.
Stability Margins (@Sensors)	SISO loop broken on measured body angular rate. Disk margins requirement.
Minimum body angular rate (p, q, r) loop gain	Body angular rate feedback loop shaping over prescribed frequency range.
Dynamic stability	Prescribed exclusion regions of Gauss plane for closed-loop eigenvalues (longitudinal and lateral-directional rigid body modes).
Body angular rate Complementary Sensitivity	Specified closed-loop frequency response from angular rate demand (model follower output) to A/C body rate (e.g. peak gain limit).
Sensitivity to Actuator Disturbance	Sensitivity function from total command disturbance to A/C body rate having gain smaller than specified threshold.
Control Moderation	Sensitivity function from filtered body rate to total stick (pedal) command having gain smaller than specified threshold.
Body Rate Gain Limit	SCAS compensator gain from filtered body rate to total stick (pedal) command shall be no bigger than specified threshold.
Body Rate Turbulence Rejection	Sensitivity from body rate disturbance to A/C body rate, multiplied by the applicable Von Karman shaping filter for severe turbulence in the given flight condition, providing sufficient gain attenuation.

Table 1: General Direct Mode SCAS CLAWs design requirements for feedback gains optimization

The optimization process is applied simultaneously to a selected number of representative HELO VTOL HOGE nominal conditions (multi-model optimization), encompassing different airspeeds, angle of sideslip, gross weight and longitudinal CG location values for the mast tilt angle equal to 90deg. Pilot's feedforward command shaping path is finally optimized based both on linear and non-linear analysis framework.

4. ASSEMBLY OF AUGMENTED LINEAR AIRCRAFT MODEL

For control laws synthesis and validation in terms of closed-loop aircraft rigid body dynamics stability and its robustness assessment, the NGCTR-TD FLIGHTLAB bare A/C linear model has to be interfaced with other aircraft subsystems linearized models, such Flight Control System (FCS), actuation, sensors, engine and drive train. The assembly procedures of relevant subsystems linear-time-invariant (LTI) state-space representations was performed using a Company developed Matlab toolbox which allows to build-up the NGCTR-TD augmented linear model.

4.1. Bare aircraft linear model

For each non-linear model (nominal and perturbed ones) and trim condition of interest, FLIGHTLAB software calculates the Jacobian matrices needed to define the bare A/C state space transformation. The linear model is initially full-order, including more than 60 states, encompassing not only canonical fuselage rigid body states but also those related to prop-rotors' gimbal flapping and aerodynamic inflow models. Based on Leonardo Helicopters experience on tiltrotor flight dynamics modelling and control, the original state vector can be reduced, whilst still ensuring accurate rigid-body dynamic predictions, to the classical flight mechanics 8 dof approximation (linear velocities u, v, w and angular rates p, q, r in body frame, roll and pitch attitude angles ϕ, θ) adding also the inertial position z (necessary to retain an accurate representation of IGE effects on bare aircraft dynamics):

$$\boldsymbol{x}=[u,v,w,p,q,r,\phi,\theta,z]$$

Once the states to be retained are chosen, the reduced order LTI system is obtained by using straightforward static condensation method (a.k.a. "slow-fast" decomposition).

In order to appreciate qualitatively the entity of the applied bare A/C perturbations in terms of reduced order linear model frequency responses, in Figure 1 and Figure 2 are showed for an example condition (WCG2, hovering, h/D=0.9), respectively the Bode magnitude and phase plot, of nominal and all perturbed models transfer functions from longitudinal (symmetric longitudinal pitch SLP), lateral (differential collective pitch DCP) and pedal (differential longitudinal pitch DLP) to A/C angular rates (both direct and cross responses). It is evident how the perturbed frequency responses are in general close to the nominal ones (almost undistinguishable), except for particular input/output couple where the spread in quite wide but only in the low frequency range: it can be justified recalling that the highest bare A/C model perturbations were applied on the parameters governing the ground effect modelling (see Section 2), which mainly influence the low frequency response of the aircraft. In order to quantify the distance between the nominal model and each perturbed version, the ν-gap metric (Ref. [17]) can provide a valid indication. The metric values satisfy 0 ≤ ν-gap ≤ 1. Values close to 0 imply that any controller stabilizing the nominal model also stabilizes an uncertain (perturbed) one with similar closed-loop gains, on the contrary if ν-gap tends to 1. The ν-gap computation was performed in the SISO way, hence for each perturbed model and each input/output couples (between the 3 commands and the 3 angular rates), and frequency-wise. The formulation is the following:

$$\delta_\nu(P_1, P_2) = \sup_\omega \psi(P_1(j\omega), P_2(j\omega))$$

$$\psi\big(P_1(j\omega), P_2(j\omega)\big) = \frac{|P_1(j\omega) - P_2(j\omega)|}{\sqrt{1 + |P_1(j\omega)|^2}\sqrt{1 + |P_2(j\omega)|^2}}$$

where, $\delta_\nu(P_1, P_2)$ is the ν-gap scalar value between the LTI systems P_1 (nominal) and P_2 (perturbed), as the supremum value along the frequency of the quantity $\psi\big(P_1(j\omega), P_2(j\omega)\big)$ computed pointwise in the frequency domain. The obtained results, for the same example case considered for the previous Bode plot, are presented in Figure 3. It can be observed how the ν-gap value is below to 0.1 (expected negligible impact of uncertainties on closed-loop stability) for all the perturbed models considering the longitudinal to pitch rate response, lateral command to roll rate, pedal to yaw rate and to roll rate. On the contrary for certain perturbed models assume closer to 1 values on the lateral command to pitch rate response, indicating closed-loop stability highly affected by uncertainties. In the other cases the ν-gap is averagely 0.2÷0.3, indicating non-negligible effects. It is worth to remark that ν-gap gives the worst case (conservative) scenario: when the actual control loop will be applied the effect of the uncertainties on stability robustness should be lower (higher gain/phase margins).

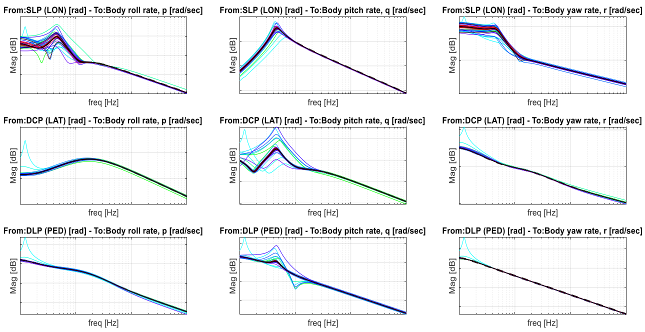

Figure 1: Bare A/C linear nominal model (dashed dark bold line) vs all perturbed ones Bode magnitude plot from commands to A/C angular rates (WCG2, hovering, h/D=0.9)

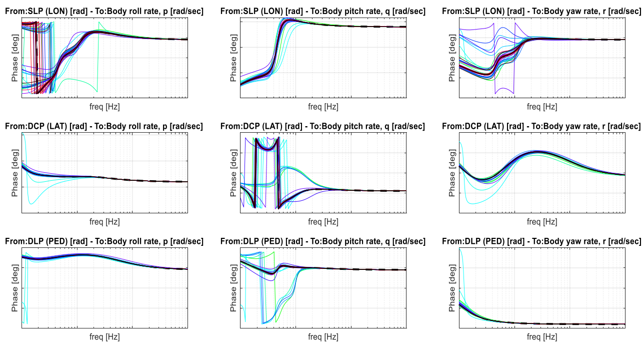

Figure 2: Bare A/C linear nominal model (dashed dark bold line) vs all perturbed ones Bode phase plot from commands to A/C angular rates (WCG2, hovering, h/D=0.9)

In Figure 4 is presented the root-locus of the reduced order bare A/C models comparing the nominal with the family of uncertain (perturbed) ones, indicating the mode shape for each eigenvalue: it's possible to appreciate qualitatively the spread of each mode due to the perturbations. The assignment of mode shape is based on the Modal Participation Factor (MPF) computation. The adopted MPF formulation, given in Ref. [11], is the following one

$$p_{ki} = \frac{|v_{ki}||w_{ki}|}{\sum_{k=1}^{n}|v_{ki}||w_{ki}|}$$

where: p_{ki} is the MPF of the i-th mode in the k-th state (n is the number of states), w_{ki} is the right eigenvectors matrix, v_{ki} is the left eigenvectors matrix. The sum of the MPF of each state to a certain eigenvalue (mode) is equal to 1: the mode shape is assigned analyzing how is distributed the modal participation along the rigid body states.

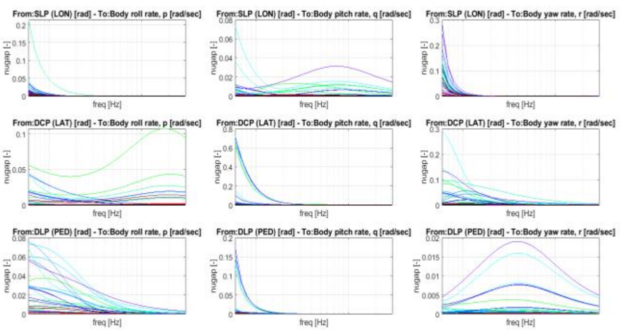

Figure 3: ν-gap metric frequency-wise computation SISO approach (from commands to A/C angular rates) between bare A/C linear nominal model and all perturbed (WCG2, hovering, h/D=0.9)

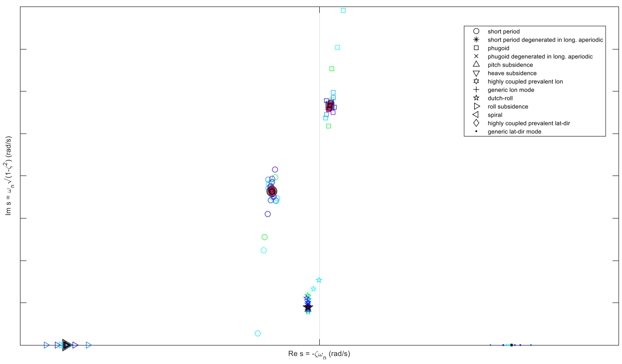

Figure 4: Bare A/C root-locus nominal model (big gray marker) vs all perturbed ones (WCG2, hovering, h/D=0.9)

It can be observed the peculiar presence of relatively fast unstable generic lateral-directional aperiodic mode (on nominal model and all perturbed ones), characterizing the HIGE bare A/C dynamics of the NGCTR-TD (thoroughly discussed in Ref. [3]): in order to stabilize it emerged the necessity to include in the CLAWs a small authority pseudo-integral term on the directional axis.

4.2. Flight Control System linear model

The control laws algorithms are modelled by means of analytical linearization of original non-linear airborne software counterpart, including FCS processing layer (e.g., input signals filtering, computational delays). The sensors, such as body angular rate and attitudes (AHRS), air data, engine (FADEC) and drive system data, are modelled by considering the equivalent dynamic response (i.e. low-pass filter) and transport delay associated to each signal. Control loop uncertainties (such as additional transport delays and or processing round-off errors acting as gain perturbations) are not included, because reasonably accounted for by stability margins (robust stability criteria).

Concerning the actuation, namely prop-rotors swashplate collective and longitudinal cyclic actuators only for the considered helicopter mode initial configuration of the NGCTR-TD, are modelled in the linear domain by means of transfer functions (i.e. low-pass filter) relating small-amplitude CLAWs command with Ram position. Nevertheless, in order to improve the reliability of the robustness analysis, also perturbed actuation models (specifically upper and lower tolerance response models with respect to nominal) have been defined, based on actuators technical specifications. The comparison of nominal and off-nominal frequency responses against specified gain and phase boundaries is reported in Figure 5 and Figure 6 for collective and longitudinal actuator, respectively.

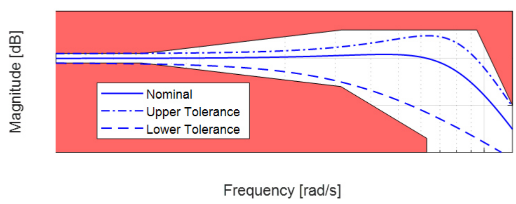

Figure 5: Nominal and off-nominal prop-rotor longitudinal cyclic pitch actuator frequency response

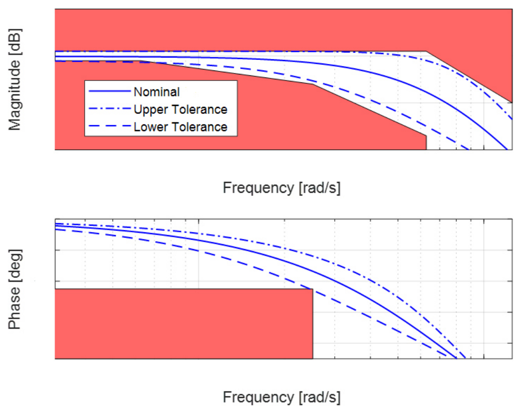

Figure 6: Nominal and off-nominal prop-rotor collective pitch actuator frequency response

4.3. Power-plant and drive-train linear model

The nacelle mounted General Electric CT7-2E1 turboshaft model is obtained via a software provided by GE Aviation running in Matlab that allows to extracting the NGCTR-TD power-plant linear state space transformation corresponding to a given operating condition, defined by required individual prop-rotor power, airspeed, pressure altitude, air temperature and NP reference speed. The power-plant linear model is fed with power demand input and power turbine speed variation and produces a single output consisting in the provided engine gas torque. Differently from bare aircraft model, which is heavily affected by uncertainties, the power-plant model is not requiring to build up a database of perturbed models. In fact, the manufacturer, based on engine deck data, ensures validation of thermodynamic derivatives. Moreover, the power-plant dynamic response is weakly coupled with overall rigid body stability and typically tolerating relatively large phase delays on Flight Control System engine command path before reducing stability margins down to a critical level.

Since the present analysis is focusing on rigid body aircraft stability (i.e. up to First Aeroelastic Mode frequency), the drive train stability characteristics will be assessed by using a rigid drive train modelling assumption which, in the NGCTR-TD case, is valid up to first torsional mode frequency. From the single dof lumped polar inertia and torsional stiffness dynamic model representing the transmission scheme, rearranged in state space form, the equivalent polar inertia J_{eq} of drive system can be extracted by noting that, in Laplace domain, it can be computed as the DC gain of engine gas torque to power turbine acceleration transfer function:

$$J_{eq} = 1/\lim_{s\to 0}\frac{s \cdot NP(s)}{Q_{gas}(s)}$$

which in turn can be used to define the rigid drive-train state space matrices:

$$A = 0, B = \left[{}^{1}\!/_{J_{eq}}\, I_{1\times 2} \quad {}^{k_{gr}^{-1}}\!/_{J_{eq}}\, I_{1\times 2}\right]$$

where the drive train model input are the engine and rotors' torque $[Q_{gas,L}, Q_{gas,R}, Q_{rot,L}, Q_{rot,R}]^T$, and the integer k_{gr} corresponds to the total gear ratio present between engine output shaft and rotor shaft.

5. ANALYSIS METHODOLOGY

The augmented aircraft linear models database, including the nominal and perturbed dynamic LTI models for each trim conditions covering hover/near hover IGE operations, built as described in the previous section, will include (depending on the analysis involved):

- Closed-loop A/C transfer functions (in state space matrix form), suitable for dynamic stability assessment (through eigenstructure and MPF analysis)
- Open-loop A/C transfer functions (SISO, one loop open at a time, or MIMO transfer matrix) open at the desired location (sensors or actuation commands), for robust stability assessment (through disk margin)

Analysis of overall perturbed bare A/C models, considering all the trim conditions and including all the permutations associated to nominal, upper tolerance and lower tolerance actuation model, would involve about 65000 LTI models, which does not appear as a practical objective. As a consequence, stability and robustness analysis were performed on the database with only bare A/C uncertainties (about 8000 LTIs), nominal actuations and also considering ideal engine/drive train. Power-plant dynamics has a minor impact on rigid body stability, therefore only on the nominal bare A/C LTI models (with nominal actuation) the stability assessment including engine and drive train models is verified.

The impact of actuation performance spread on closed-loop A/C stability will be analyzed by combining the worst-case conditions found from the above analysis considering only the bare A/C uncertainties, with the perturbed actuation models. In particular for each of the 3 W/CG conditions considered, 3 worst cases were selected:

- from closed-loop dynamic stability analysis, the perturbed model and trim condition having the worst periodic mode (highest eigenvalue real part) along the whole database
- from closed-loop dynamic stability analysis, the perturbed model and trim condition having the worst aperiodic mode (highest eigenvalue real part) along the whole database
- from robust stability analysis, the perturbed model and trim condition having the worst stability margins (lower gain/phase margins) along the whole database

For each of the resulting 9 worst conditions the various swashplate actuators perturbation combination listed in Table 2 are considered, for total resulting additional 72 test conditions to be evaluated in terms of both dynamics stability and its robustness.

Case	Collective Actuator	Longitudinal Actuator
1	Nominal	Lower Tolerance
2	Nominal	Upper Tolerance
3	Lower Tolerance	Nominal
4	Upper Tolerance	Nominal
6	Lower Tolerance	Lower Tolerance
7	Lower Tolerance	Upper Tolerance
8	Upper Tolerance	Upper Tolerance
9	Upper Tolerance	Lower Tolerance

Table 2: Combination of swashplate actuator models for robust stability assessment

5.1. Dynamic stability analysis

For each LTI model of the database, the state matrix eigenvalues are computed and analyzed, using the Modal Participation Factor technique to identify the modes shape also for the closed-loop case. Respect to the bare A/C MPF analysis, the closed-loop system is characterized by a higher number of states (and then eigenvalues), introduced by FCS, actuators, sensors, engine and drive train, in addition to the 9 rigid body states of the reduced order bare dynamics. All the closed-loop system eigenvalues having a total modal participation on rigid body states below a 0.1 imposed threshold is deemed negligible in terms of rigid body participation and then not considered in the A/C stability analysis. Only eigenvalues having a total modal participation on rigid body states above the threshold are considered and checked with respect to dynamic stability requirements.

The dynamic stability prescription given in FAR TR.181(c) are considered (which are in turn from Ref. [18] MIL-H-8501A IFR boundaries), defining a unique limit for both longitudinal and lateral-directional modes in closed-loop for tiltrotor in VTOL/Conversion mode. In case of either marginal compliance or small deviations from TR.181 (especially with perturbed models), the possible application of less conservative VFR dynamic stability requirement from MIL-H-8501A can be considered, in particular taking in mind the initial phase of NGCTR-TD flight test activities, limited to hover/near hover in ground effect operations. As ultimate least conservative stability limit the Ref. [19] ADS-33 Level 2 boundary can be adopted. In Figure 7 the cited limits are compared. It is worth to note that MIL-H-8501A VFR does not define limitation for frequencies below ~0.3rad/s and for aperiodic modes.

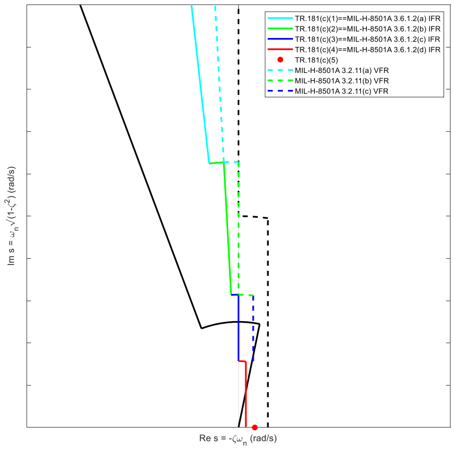

Figure 7: Comparative study of available VTOL/Conv. mode dynamic stability requirements

5.2. Robust stability analysis

The robust stability consist in computing the gain and phase margins of the open control loop. Canonically the gain margin is the amount of gain variance required to make the feedback loop gain unity at the frequency where the phase angle is -180deg. Similarly, the phase margin is the difference between the phase of the response and -180deg when the loop gain is equal to 1 (0 dB). The gain margin measures the amount of allowable perturbation in the plant gain before the closed loop become unstable, which corresponds to real perturbations, while the phase margin is the amount of allowable variation in the plant phase before the closed-loop becomes unstable, which corresponds to phase perturbation. Hence gain and phase perturbation are applied separately. These definitions are straightforward for a SISO system and can be simply extended to assess the robustness of a MIMO feedback system by means of the loop-at-time analysis: margins are computed introducing perturbations in a single channel by breaking one loop at time with all other loops closed. But the canonical approach to gain/phase margin computation presents two main limitations:

- real systems differ from their mathematical models in both magnitude and phase simultaneously

- a MIMO feedback system can have large loop-at-time margins and yet be destabilized by small perturbations acting simultaneously on multiple channels

In the present work was preferred to adopt the disk-based stability margins method (Ref. [13]) for the robustness assessment: instead of the canonical one it considers a concurrent perturbation on both gain and phase and on all the channels of the control system at the same time. Hence provides a stronger guarantee of closed-loop stability than the classical gain and phase margins. The most significant characteristics of the two methods are summarized in Table 3.

Classical Approach	Disk Margin Approach
Complex perturbations (gain & phase) to represent simultaneous gain and phase variations are not used.	A general family of complex perturbations to represent simultaneous gain and phase variations is used.
Loop-at-a-time analysis fails to capture the effect of simultaneous perturbations occurring in multiple channels (MIMO) systems.	Separate, independent gain/phase variation in multiple channels can be taken into account.
Reduced information regarding the impact of model uncertainties (only in two frequency points).	Additional information regarding the impact of model uncertainties at various frequencies.
Overly optimistic assessment of the system robustness.	A more realistic assessment of the system robustness can be done.

Table 3: Differences between classical and disk criterion approach to stability margins computation

Without entering in the mathematical details needed to fully present the disk margin computing in the MIMO case, hereafter are showed some highlights of the formulation for the SISO one, enough to appreciate its meaning. Considering a generic SISO negative feedback control loop depicted below

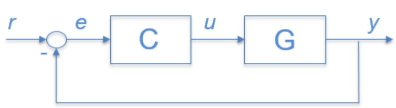

the open-loop transfer function is defined as

$$L(s) = C(s)G(s)$$

For SISO $L(s)$, the uncertainty model for disk-margin analysis incorporates a multiplicative complex uncertainty Δ into the loop transfer function as follows

$$L \rightarrow L_\Delta = L\frac{1+\frac{\Delta(1-E)}{2}}{1-\frac{\Delta(1+E)}{2}} = L(1+\delta_L), \quad |\Delta| < \alpha$$

When $\Delta = 0$, the multiplicative factor is 1, corresponding to the nominal L. As Δ varies in the ball $|\Delta| < \alpha$, the factor $L(1+\delta_L)$ varies in a disk. The gain and phase of the factor are a model for gain and phase variation in L. The eccentricity parameter E varies the shape of the disk, hence the shape of the applied uncertainty in the complex plane. The disk margin is the smallest value of α at which the closed-loop system becomes unstable. The shaded region in Figure 8 shows the range of $(1+\delta_L)$ values in the complex plane for $|\Delta| < \alpha$ and fixed E. The gain margins $[g_{min}, g_{max}]$ are the points where the disk intercepts the real axis. The gain can vary by any factor in this range without compromising stability. The phase margin is the largest angle ϕ_{max} that any point in the disk makes with the real axis. The system can tolerate changes in phase of $\pm\phi_{max}$.

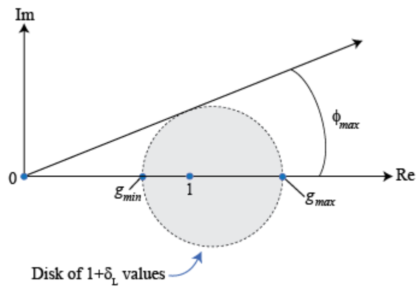

Figure 8: Disk-based margins geometrical interpretation

With this uncertainty applied to L, the closed-loop system remains stable for all $|\Delta| < \alpha$ when, for all frequencies ω

$$\left|S(j\omega) + \frac{E-1}{2}I\right| < \frac{1}{\alpha}$$

where S is the sensitivity function $(I+L)^{-1}$. In other words, α can be computed from the peak gain of a shifted sensitivity function

$$S + \frac{(E-1)I}{2}$$

The eccentricity parameter E in the default algorithm (as considered hereafter) in equal to 0, which corresponds to the balanced sensitivity function

$$S - \frac{I}{2} = \frac{S - F}{2}$$

where, $F = I - S$ is the complementary sensitivity function.

Finally, from the smallest value $\bar{\alpha}$ at which the closed-loop system becomes unstable, the minimum guaranteed gain and phase margins are computed as follow:

$$g_{min} = \frac{2 - \bar{\alpha}(1 - E)}{2 + \bar{\alpha}(1 + E)} \ ; \ g_{max} = \frac{2 + \bar{\alpha}(1 - E)}{2 - \bar{\alpha}(1 + E)}$$

$$\phi_{max} = \cos^{-1}\left(\frac{1 + g_{min}g_{max}}{g_{min}g_{max}}\right)$$

$$Gain\ Margin: GM_{dB} = [\min(1/g_{min}, g_{max})]$$
$$Phase\ Margin: PM_{deg} = \phi_{max}(180/\pi)$$

The above $\bar{\alpha}$ corresponding parameters $[\,g_{min}, g_{max}, \phi_{max}]$ and then disk-based gain/phase margins, are computed frequency-wise: the actual stability margins of the system are the minimum values of GM and PM along the frequency range of interest. The extension for MIMO system is obtained with an analogous uncertainty model applied to L that allows the uncertainty to vary independently in each channel.

For each entry of the augmented aircraft linear models database, including the nominal and perturbed dynamic LTI models for each trim conditions, the disk margin SISO computation (loop-at-a-time) was performed:

- opening the loop at each sensor interface, hence considering the L function from each angular rate reference of the CLAWs SCAS to corresponding angular rate

$$L_{p_{ref}\to p}\ ;\ L_{q_{ref}\to q}\ ;\ L_{r_{ref}\to r}$$

- opening the loop at each actuation interface, hence considering the $L(s)$ function from each command reference of the CLAWs SCAS to corresponding command

$$L_{LAT_{ref}\to LAT}\ ;\ L_{LON_{ref}\to LON}\ ;\ L_{PED_{ref}\to PED}$$

Also the MIMO disk margin was computed, considering in this case:

- at sensor interface opening the transfer matrix

  L 3x3 from $(p, q, r)_{ref}$ to (p, q, r)

- at actuation interface opening the transfer matrix

  L 3x3 from $(LON, LAT, PED)_{ref}$ to (LON, LAT, PED)

Hereafter, the requirements from SAE-AS-94900 adopted as reference for the robust stability assessment are briefly recalled. When the classical rigid body A/C closed-loop dynamic stability assessment is considered, the requirements are applicable up to the First Aeroelastic Mode (FAM), excluding any airframe/FCS structural coupling. A lower value of acceptable gain and phase margin is prescribed for frequencies f_M below 0.06Hz, while higher limits (more robustness required) are defined above this threshold, up to the FAM. These margins are intended to be applied when model uncertainties are not taken into account. For perturbed (i.e. off-nominal, uncertain) FCS loops, the SAE-AS-94900 allows a reduction up to 50% of the nominal limits. It is worth to remark that the standard suggest to perform the assessment of control robustness to aerodynamic uncertainties using variations on critical stability derivatives, determined by the data source and its fidelity, of at least ±20%: a value largely exceed for certain model parameters perturbation as discussed in Section 2, typically the ones associated to the ground effect modelling.

The SAE-AS-94900 boundaries are defined accordingly to the classical approach to compute gain and phase margin, namely:

- GM (Gain Margin): the change in loop gain required to reach unity loop gain (0 dB), at the frequency where open loop phase is at -180 degrees
- PM (Phase Margin): the change in open loop phase required to reach -180 degrees phase in open loop at the frequency where the open loop gain crosses unity
- f_M : the lowest Frequency in Hz where the loop gain crosses 0 dB (phase margin crossover) or open loop phase crosses -180 degrees (gain margin crossover)

and, for multiple control loop system, by opening one loop at a time.

However, it is also possible to compute gain and phase margins using the modern disk margin method previously discussed, where a simultaneous perturbation of both gain and phase (hence a complex perturbation) is applied to the closed loop system. The disk margin approach can be computed opening one loop at a time (SISO) or considering the MIMO system. Already with the SISO approach a first level of conservativism in the computation (lower margins obtained) is added respect to canonical definition. In the MIMO way the complex perturbation is applied simultaneously on all the control loops, resulting in the worst case (i.e. lowest margins) results, adding a further amount of conservativism. Taking in mind these consideration, the gain/phase margins requirements given in the SAE-AS-94900 should be slightly relaxed when disk SISO approach is adopted or eventually used as is but critically evaluating eventual non-compliances. While when the MIMO approach is used, the computation approach is too different to the canonical stability margins definition on which the SAE limits are defined, and they become inapplicable as is. Therefore, for the robustness assessment of the NGCTR-TD the disk SISO computation was preferred, in order to consider still meaningful the SAE limits.

5.3. Disk margin applicability criteria

It should be noted, as thoroughly discussed hereafter, that the processing of disk-based stability margins is not well posed at frequencies corresponding to unstable modes. However, provided that TR.181(c)(4) stability requirement is met, no aperiodic unstable mode should exist above ln(2)/9 = 0.077rad/s i.e. 0.012Hz, whereas lower frequency bound prescribed by SAE-AS-94900 for most demanding GM/PM target is higher (0.06Hz or 0.38rad/s). Consequently, verification of the mid-frequency range robust stability requirement should be done also in presence of closed-loop unstable A/C, as it is possible adopting a specific approach in the choice of the frequency range along which the disk margins are evaluated, based on closed-loop system eigenvalues placement. This is, for sure, the key aspect and the novelty of the developed robust assessment analysis methodology. The upper limit of the disk margin computation frequency range is placed equal to the First Aeroelastic Mode (FAM) frequency of the NGCTR-TD, since the A/C closed-loop dynamic stability assessment is limited to the rigid body. While the lower frequency bound is chosen accordingly to the devised following criteria:

- If the considered closed-loop model and trim condition from dynamic stability analysis is stable the disk margins are evaluated using a lower frequency bound corresponding to the stable mode with lowest frequency
- If the considered closed-loop model and trim condition from dynamic stability analysis is unstable, the two following cases are distinguished:
  - if there is only one rigid body mode unstable, detect its frequency f_{unst} and search along the stable modes (ordered by increasing frequency), the first one having the frequency $f_{stab\,1}$ greater than $TOL \cdot f_{unst}$. The disk margins are computed using a lower frequency bound corresponding to $f_{stab\,1}$.
  - if there is more than one rigid body mode unstable, detect the one with the highest frequency $f_{unst\,MAX}$ and search along the stable modes (ordered by increasing frequency), the first one having the frequency $f_{stab\,2}$ greater than $TOL \cdot f_{unst\,MAX}$. The disk margins are computed using a lower bound equal to the frequency of the stable mode $f_{stab\,2}$.

The tolerance TOL allows to set a further gap respect to unstable mode frequency for searching the first stable one, and thus the lower frequency bound for disk margins computing. Since disk-based stability margins are not well posed at frequencies corresponding to unstable modes, the above criteria defines a disk margin computing exclusion area in terms of lower bound frequency: a semi-circle on the Gauss plane, delimited by the iso-frequency line at $TOL \cdot f_{unst}$ (or $TOL \cdot f_{unst\,MAX}$). The TOL value was set equal to 2, deemed enough to consider reliable the disk margins evaluation. In other words, while in canonical sense the stability margins are null by definition for an unstable system, the disk margins approach consents to have a measure of system robustness also in this case, but only placing the lower frequency bound of computation sufficiently above the unstable modes frequency, to avoid the stability margins drop bias due to their presence.

To better understand the approach, some examples are provided. In Figure 9 is depicted the root-locus of a closed-loop stable case: the lowest frequency mode is a phugoid degenerated in aperiodic, therefore the disk margin lower bound computing frequency was chosen equal to this mode frequency, represented by the cyan vertical line in Figure 10, showing the disk-based margins results along the frequency range considered, up to FAM. The resulting gain and phase margin values are the minimum ones registered on the frequency range: in the reported example the margins drop occurs below the 0.06Hz threshold specified by the SAE-AS-94900 under which the GM/PM required values are relaxed, and the robustness requirement is barely satisfied.

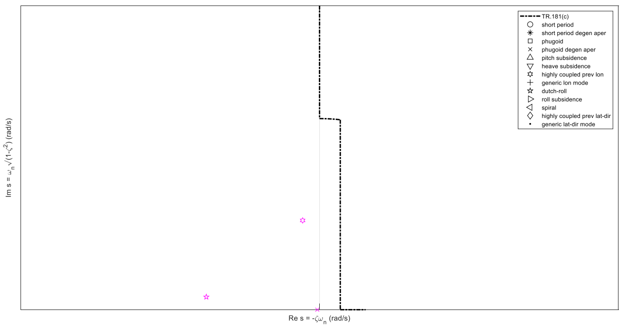

Figure 9: Root-locus nominal model closed-loop, WCG2, AoS=90deg, KCAS=10, h/D=1.2: example of stable system

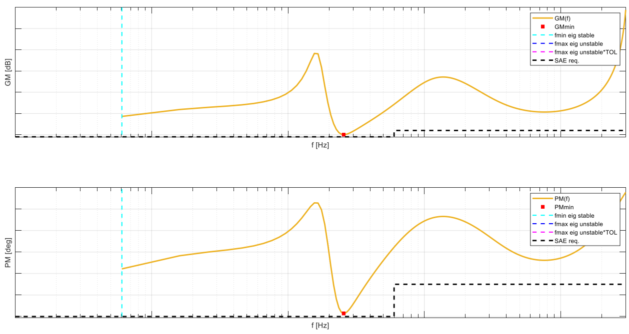

Figure 10: Disk-based gain and phase margin frequency-wise, WCG2, AoS=90deg, KCAS=10, h/D=1.2, loop open on pitch rate: example of stable system

In Figure 11 is depicted the root-locus of a closed-loop unstable case: there is a single eigenvalue on the right half of Gauss plane, in particular an aperiodic generic lateral-directional mode, compliant with the TR.181(c) requirement, hence below 0.012 Hz. Accordingly to the developed criteria, the exclusion area boundary for the disk computation is traced with the dotted red iso-frequency (2 times the unstable mode frequency) semi-circle on the Gauss plane. Into the exclusion area falls another generic lateral-directional mode but stable, while the first stable eigenvalue (lowest frequency) outside the area is a phugoid. In Figure 12 and Figure 13 are presented the disk-based margins results along the frequency range considered, up to FAM, for this unstable case example, respectively with the loop opening on sensor roll rate and pitch rate. The blue vertical line indicates the unstable mode frequency, magenta one the exclusion limit (at 2 times the unstable mode frequency) and with the cyan is marked the lowest frequency stable mode beyond the exclusion zone, from which the disk computation is evaluated. In Figure 12 can be appreciated the difference in gain/phase margin results (in terms of both frequency and value) when the minimum is taken from the cyan line frequency (red square marker) accordingly to the adopted criteria, respect to starting the disk computing at a frequency such as to include the unstable mode (resulting minimum GM/PM depicted with dark circle marker). It is evident the stability margins drop bias due to the unstable mode presence and the extension of its effect along the frequency. Evidently the absolute minimum of gain/phase found is not of interest for the robustness evaluation because at a frequency where the system in unstable and then definition of stability margin is not applicable. While the developed criteria allows to extract a meaningful measure of the robustness, in the frequency range of interest for the control.

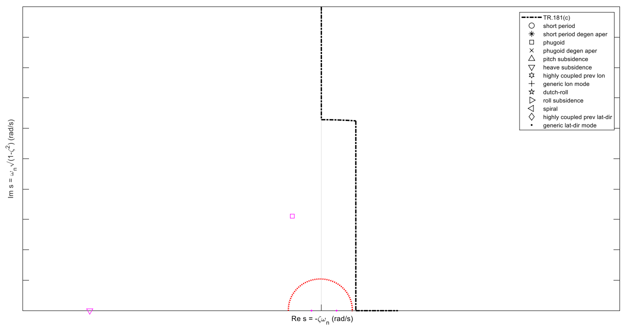

Figure 11: Root-locus nominal model closed-loop, WCG2, AoS=0deg, KCAS=15, h/D=0.7: example of unstable system

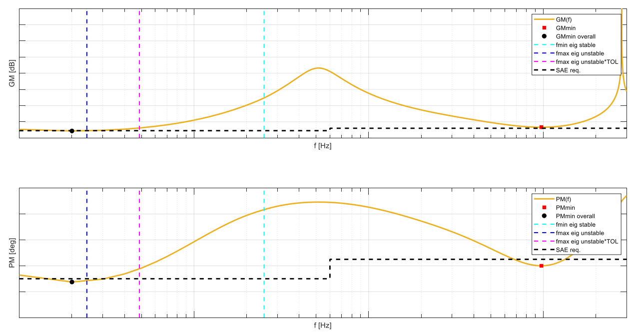

Figure 12: Disk-based gain and phase margin frequency-wise, WCG2, AoS=0deg, KCAS=15, h/D=0.7, loop open on roll rate: example of unstable system

The Figure 13 shows the same evaluation for the pitch rate loop opening: in this case absolute and local GM/PM minimum are coincident, exactly at the frequency of the first stable mode beyond the exclusion zone.

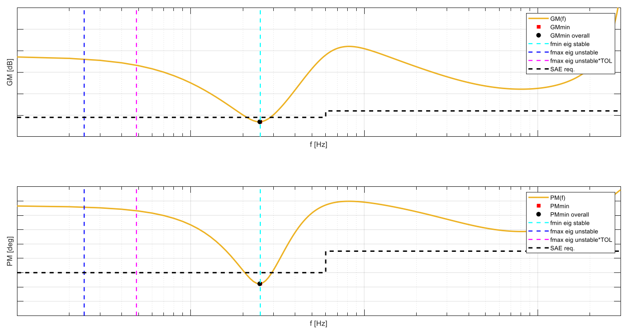

Figure 13: Disk-based gain and phase margin frequency-wise, WCG2, AoS=0deg, KCAS=15, h/D=0.7, loop open on pitch rate: example of unstable system

Finally, it is worth to observe a sort of dichotomy between the dynamic stability requirements of TR.181 for tiltrotor in VTOL/Conversion mode and robustness requirements of SAE-AS-94900. While the presence of unstable modes (with time to double higher than 9sec, i.e. frequency lower than ln(2)/9 = 0.077rad/s = 0.012Hz) in closed-loop is allowed, positive stability margins defined in the canonical sense are requested, when are null by definition for an unstable system. This is another rationale to prefer the disk margins approach for the robustness assessment, which consents to deal also with unstable dynamics, enforcing the appropriate precautions above illustrated.

6. ANALYSIS RESULTS

In this section is presented and discussed a selection of the results obtained from the conducted analysis, applying the described methodology to the NGCTR-TD. First, the dynamic stability and robustness evaluation, applying only the bare A/C model uncertainties, is showed. Then, the worst cases selection is performed and the stability assessment including the actuation uncertainties is illustrated.

6.1. Stability analysis applying bare A/C uncertainties

Before investigating the effects of model uncertainties, it is useful to analyze the dynamic stability in closed-loop using the nominal model along the considered trim conditions in hover/near hover IGE. Since the minor impact of the weight and balance perturbation on the results, only the starting WCG2 (W mid, CG MID) configuration is considered. In Figure 14 are showed only the closed-loop eigenvalues non-compliant respect to TR.181(c) on the Gauss plane: each subplot represents the sensitivity to a different trim parameter (sideslip, airspeed, non-dimensional height above ground) using markers color, while the markers indicate the mode shape assignment.

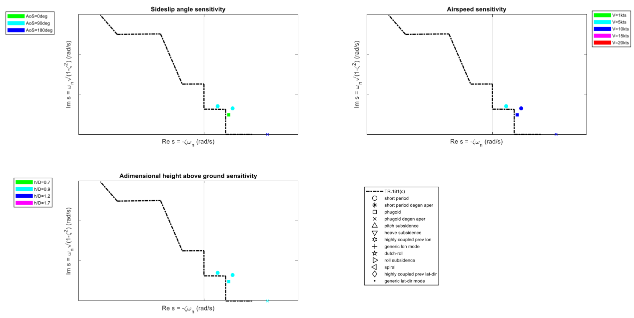

Figure 14: Root-locus nominal model WCG2 closed-loop, dynamic stability requirement deviations respect to TR.181(c), parameters sensitivity

The Figure 15 allows to appreciate how the stability deviation occurrences (in percentage respect to total) from requirements are distributed along the trim parameters and in terms of mode shape: it emerges that nominal model non-compliances involve only longitudinal modes, a specific height above ground (h/D=0.7) and two airspeed conditions (5 and 10kts), while all the sideslip angles are affected, but prevalently the sideward flight. The detected stability non-compliances for the nominal model are close to the requirement boundary, as quantified in Figure 16, where the occurrences are grouped by unstable mode time to double: the majority have double time higher than 9 seconds, some cases between 5 and 9sec. and none below 5sec.

Now moving to the uncertain (perturbed) models, the dynamic stability results are presented in a similar graphical fashion, showing for instance only the WCG3 condition (W mid plus delta W, CG MID with forward delta): no significant sensitivity to weight and balance perturbation emerged, as for the nominal model. In Figure 17 are showed only the closed-loop eigenvalues non-compliant respect to TR.181(c) on the Gauss plane, along all the perturbed models and trim conditions. The low-frequency deviations from TR.181(c) have been compared also against less conservative MIL-H-8501A VFR boundaries and

ADS-33 Level 2: the last one is always met, while only very few cases are beyond VFR prescription. The requirement deviation occurrences distribution is showed in Figure 18 and in general recall the same picture obtained for the nominal model in Figure 15: only longitudinal modes involved, majority of non-compliances at 10kts sideward, all at h/D=0.9.

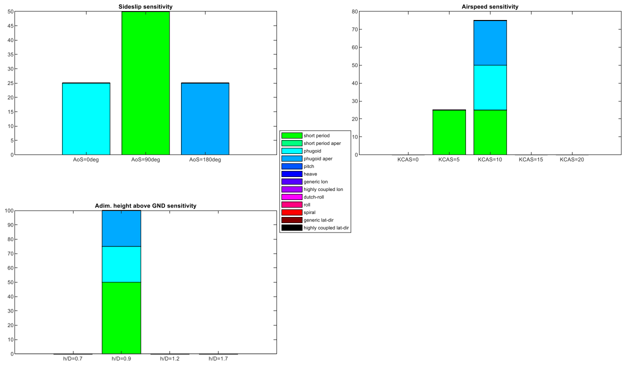

Figure 15: Nominal model WCG2 closed-loop, dynamic stability requirement deviation occurrences percentage, parameters sensitivity respect to mode shape

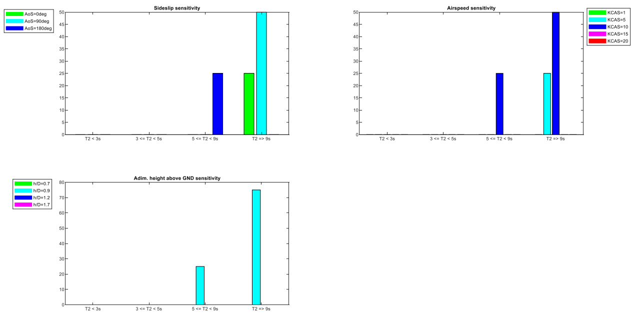

Figure 16: Nominal model WCG2 closed-loop, dynamic stability requirement deviation occurrences percentage, parameters sensitivity respect to mode double time

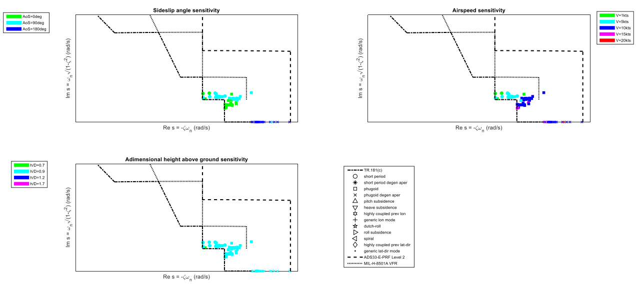

Figure 17: Root-locus perturbed models WCG3 closed-loop, dynamic stability requirement deviation respect to TR.181(c), parameters sensitivity: different requirements comparison

For the perturbed models analysis, is showed also the occurrences distribution along the perturbed models (identified by a progressive number) in the right/down subplot: it can be stated that dynamics stability non-compliances are nearly equidistributed on perturbed models, without a specific polarization on a certain type of uncertainties applied on bare A/C: it is a good statistical indicator despite the adoption of a physics based approach to create a relatively small uncertain model database, instead of the typically large one from Monte Carlo trials. Also in terms of time to double grouping, the results on perturbed models in Figure 19 are basically the same found for the nominal in Figure 16.

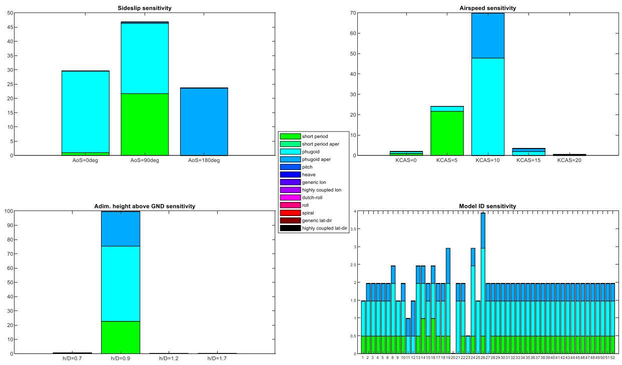

Figure 18: Perturbed models WCG3 closed-loop, dynamic stability requirement deviation occurrences percentage parameters sensitivity respect to mode shape

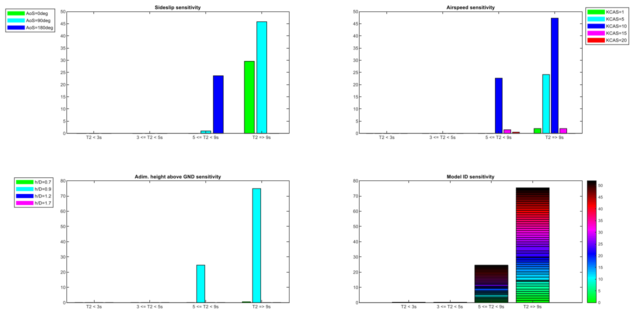

Figure 19: Perturbed models WCG3 closed-loop, dynamic stability requirement deviation occurrences percentage, parameters sensitivity respect mode double time

Considering the dynamic stability results, the NGCTR-TD in hover-near hover IGE conditions can be considered compliant with the desired requirements from a practical standpoint. Minor deviations respect to TR.181(c) at very low frequency (~0.02 Hz) for both nominal and perturbed models regardless of weight and balance configuration was found, associated to longitudinal axis unstable modes, only for h/D = 0.9. However these deviations are compliant with ADS-33 Level 2 (T2 ≤ 5.0 seconds) and MIL-H-8501A VFR specifications. These deviations are considered operatively acceptable, especially considering the degraded CLAWs configuration providing basic rate stabilization (Direct Mode) and the in ground effect flight conditions.

6.2. Robust stability analysis applying bare A/C uncertainties

First, are presented the robust stability analysis results relative to the nominal model along the considered trim conditions. In particular only the WCG2 (W mid, CG MID) is showed, considering the minor impact of the weight and balance perturbation on the results, and only opening the loop at each sensor interface, because the command interface counterpart gives practically the same outcome. The disk-based gain and phase margins are reported as a function of the frequency where the minimum occurs (by definition minimum GM and PM are at the same frequency), for each sensor loop (roll, pitch, yaw rates), using the same figure layout: each subplot represents the sensitivity to a different trim parameter (sideslip, airspeed, non-dimensional height above ground) using markers color. All the results are depicted, namely both the trim conditions compliant with SAE-AS-94900 limits and non-compliant. All the trim conditions in terms of gain margin with loop open on roll rate met the requirement, as showed in Figure 20, as well as both gain and phase margins for the yaw rate loop opening, as per Figure 24, Figure 25.

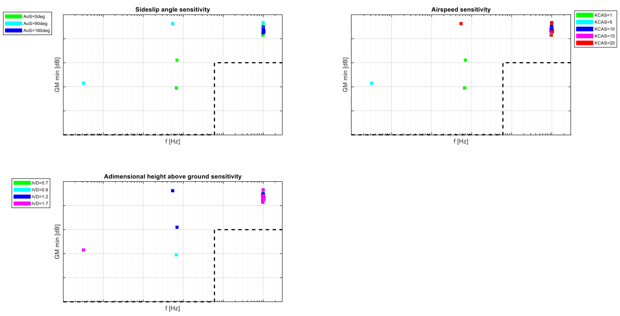

Figure 20: Disk Gain Margin of nominal model WCG2 with loop open on roll rate, parameters sensitivity

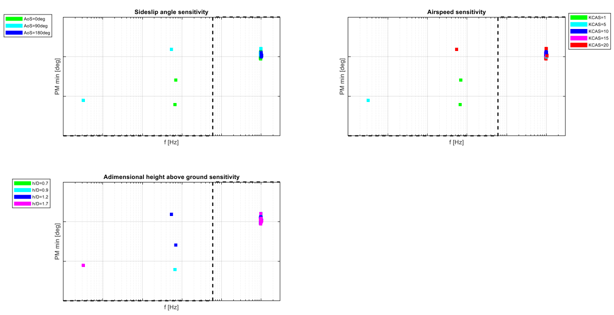

Figure 21: Disk Phase Margin of nominal model WCG2 with loop open on roll rate, parameters sensitivity

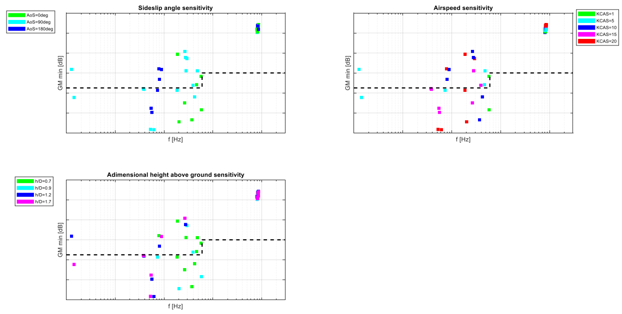

Figure 22: Disk Gain Margin of nominal model WCG2 with loop open on pitch rate, parameters sensitivity

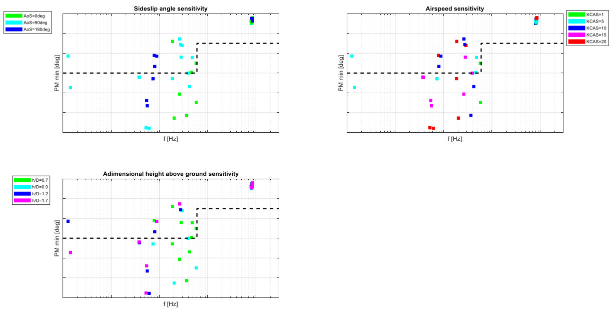

Figure 23: Disk Phase Margin of nominal model WCG2 with loop open on pitch rate, parameters sensitivity

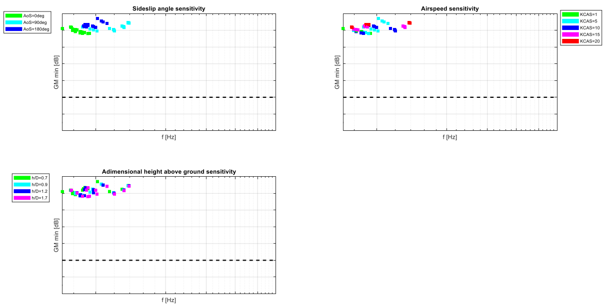

Figure 24: Disk Gain Margin of nominal model WCG2 with loop open on yaw rate, parameters sensitivity

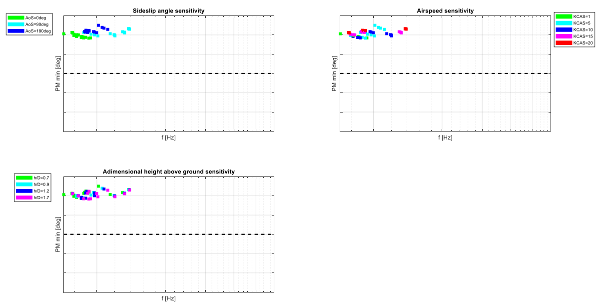

Figure 25: Disk Phase Margin of nominal model WCG2 with loop open on yaw rate, parameters sensitivity

While a certain number of trim conditions were found with disk margin (gain and phase) values well below the desired SAE limit at frequency below 0.06Hz, for the longitudinal channel, as showed in Figure 22 and Figure 23. Insufficient stability margins below 0.06Hz are not considered of any practical concern because the disk margin processing is affected by the nearby unstable modes, which are considered acceptable (up to a certain time to double) based on the dynamics stability requirements. In other words, these non-compliances at very low frequency derive from poorly harmonized dynamic and robust stability requirements. From Figure 21, only few trim cases were found with slightly not compliant disk phase margin at frequencies of interest for CLAWs loop closures (around 1Hz), for SCAS roll rate sensor feedback loop broken (and similarly for total lateral command opening). However, considering the conservativism inherently introduced by the disk margin approach, small deviations respect to the desired margins value based on canonical stability margins definition, can be reasonably accepted. In Figure 26 are showed the total non-compliances occurrences percentage distribution along the trim parameters and in terms of considered SCAS channel: as already observed none non-compliances were found on yaw sensor loop opening, while the deviations detected on pitch and roll rate loops do not show any particular polarization on specific trim conditions. Only for the roll rate sensor feedback loop broken and the phase margin, where slight deviations from requirements were detected at frequencies of interest, are reported further histograms. In Figure 27 are showed the phase margins non-compliance occurrences distribution on trim parameters and grouped in three phase margin ranges, from zero to the required SAE value.

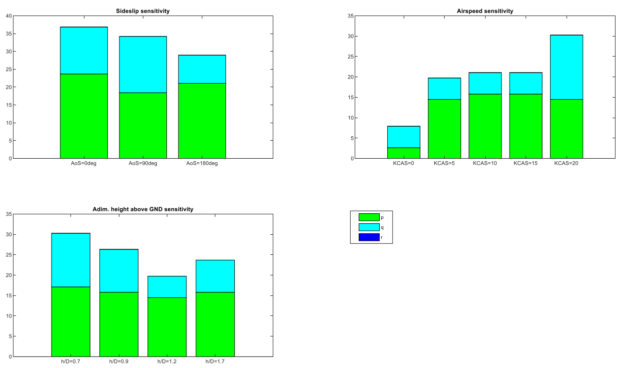

Figure 26: Disk Margin of nominal model WCG2 requirement deviation occurrences percentage (both gain and phase), parameters sensitivity respect axis (loop broken at sensors interface)

While Figure 28 shows a similar representation but with the corresponding grouping in frequency for the phase margin non-compliances: from 0 to the SAE threshold at 0.06Hz, from 0.06 to 1Hz, considered the upper limit of the frequency range of interest for control, and from 1Hz to FAM frequency.

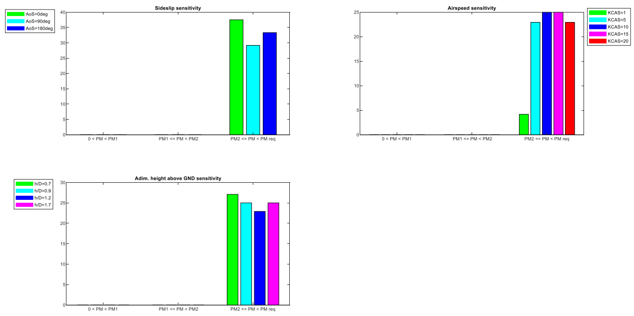

Figure 27: Disk Phase Margin of nominal model WCG2, loop open on roll rate, requirement deviation occurrences percentage, parameters sensitivity respect phase margin ranges below requirement limit

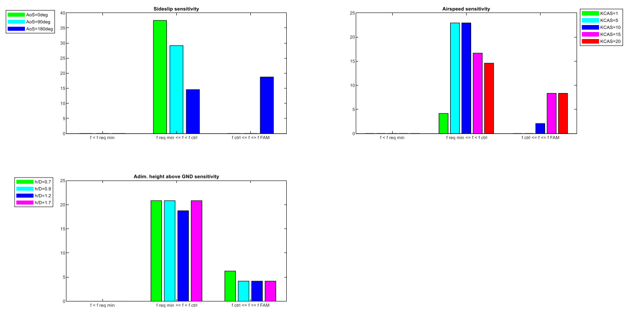

Figure 28: Disk Phase Margin of nominal model WCG2, loop open on roll rate, requirement deviation occurrences percentage, parameters sensitivity respect frequency ranges

The results overview continues with the robust stability analysis considering the uncertain (perturbed) models. In general full compliance respect to SAE requirements was verified above 0.06 Hz threshold for all loop opening positions, thanks to relaxed (50% lower) robust stability boundaries applicable to perturbed models. In general, disk margins trend observed for nominal model is confirmed, with a minor worsening caused by model perturbations. Also for the perturbed models are predicted deviations from desired stability margins below 0.06 Hz, mostly affecting longitudinal axis, and less lateral axis. Infrequent low frequency deviations associated to directional axis are most likely outliers.

For sake of brevity results are showed only for the WCG1 (W mid minus delta W, CG MID with afterward delta), because the main outcomes do not change with weight and balance perturbation. In Figure 29 the total gain and phase non-compliances percentage occurrences are illustrated along the perturbed model ID (in abscissa), using bar colors to evaluate trim parameters and channel sensitivity. As already observed on dynamics stability results, also margins non-compliances are nearly equidistributed on perturbed models, without a specific polarization on a certain type of uncertainties applied on bare A/C. In terms of channel opening, the most affected in terms of occurrences is the longitudinal one, followed by the lateral one. Very few non-compliance on directional one (fundamentally outliers). In terms of sideslip and airspeed the majority of non-compliances occur in forward and sideward flight at 15-20kts, while the most affected height from ground is h/D=1.2. Considering only loop open at roll rate sensor, because it is the channel with lower margins detected (same evidence found on nominal model), Figure 30 and Figure 31 report disk-based gain and phase margins as a function of the frequency using the same figure layout: each subplot represents the sensitivity to a different trim parameter (sideslip, airspeed, non-dimensional height above ground) and to the perturbed model ID number.

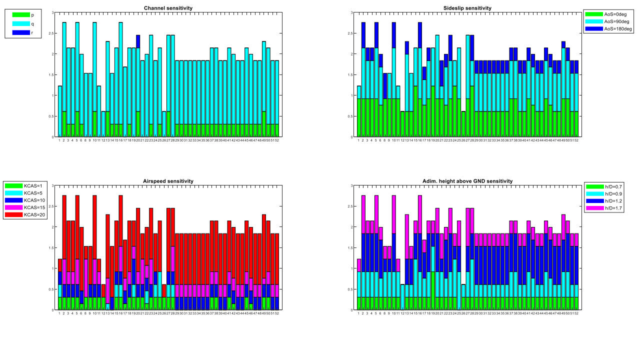

Figure 29: Disk Margin of perturbed models WCG1 requirement deviation occurrences with loop broken at sensors interface, parameters sensitivity respect perturbed model ID

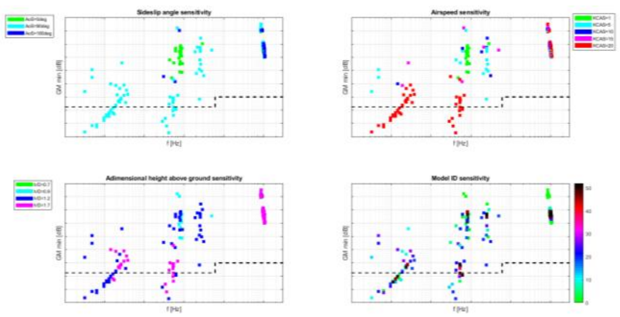

Figure 30: Disk Gain Margin of perturbed models WCG1 with loop open on roll rate, parameters sensitivity

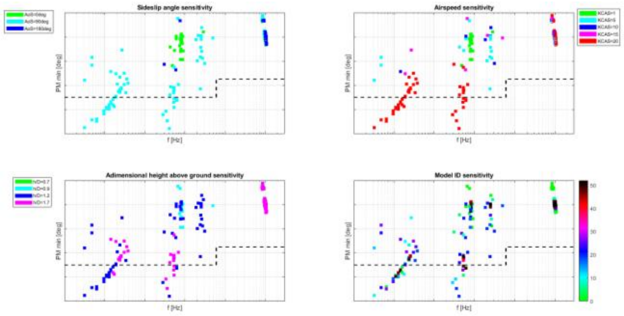

Figure 31: Disk Phase Margin of perturbed models WCG1 with loop open on roll rate, parameters sensitivity

Focusing on the phase margin non-compliances on lateral channel, where the nominal model shows slightly insufficient values around 1Hz, also on perturbed models the lowest margins occur at this loop opening, but thanks to the 50% reduction of SAE required margins the results are compliant. In Figure 32 phase non-compliances percentage occurrences distribution on trim parameters and perturbed model ID is presented, grouped in three phase margin ranges, from zero to the required SAE value.

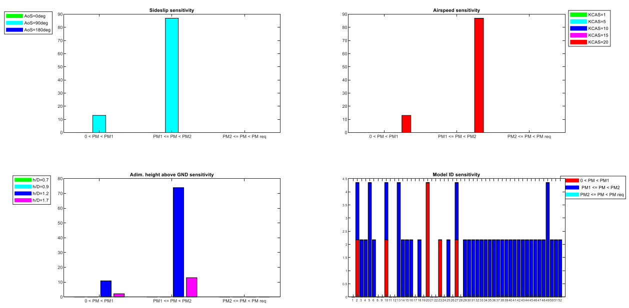

Figure 32: Disk Phase Margin of perturbed models WCG1, loop open on roll rate, requirement deviation occurrences percentage, parameters sensitivity respect phase margin ranges below requirement limit

While Figure 33 shows a similar representation but with the corresponding grouping in frequency for the phase margin non-compliances: from 0 to the SAE threshold at 0.06Hz, from 0.06 to 1Hz, and from 1Hz to FAM frequency. It's possible to state again that non-compliances are almost equidistributed along the perturbed models, while occur totally in sideward flight at 20kts and mainly at h/D=1.2. In terms of phase margin values the most are in the middle range and always at frequency below 0.06Hz.

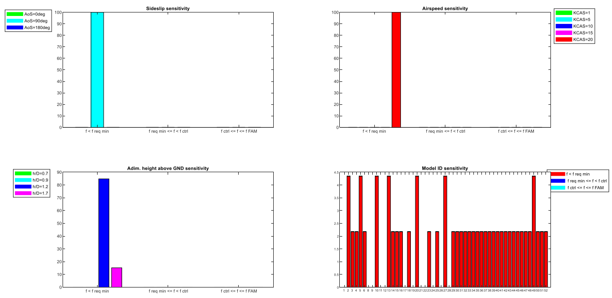

Figure 33: Disk Phase Margin of perturbed models WCG1, loop open on roll rate, requirement deviation occurrences percentage, parameters sensitivity respect frequency ranges

Bearing in mind the emerged evidence of reduced SISO disk-based phase margins of lateral control channel at approximately 1 Hz, a further investigation was conducted, computing the conventional SISO stability margins. The outcome is a full compliant picture respect the SAE requirements, as expected considering the inherent conservativism of disk margins computation respect the canonical one. An example is reported in Figure 34, showing the conventional margins for the WCG1 perturbed models, roll rate loop opening, and all the trim conditions: the blue line depict the combined gain/phase margins SAE requirement (for nominal model) above 0.06Hz threshold, the yellow the limits below it. The results are all compliant respect to the higher margins target, despite the perturbed models are considered, for which the relaxation can be applied.

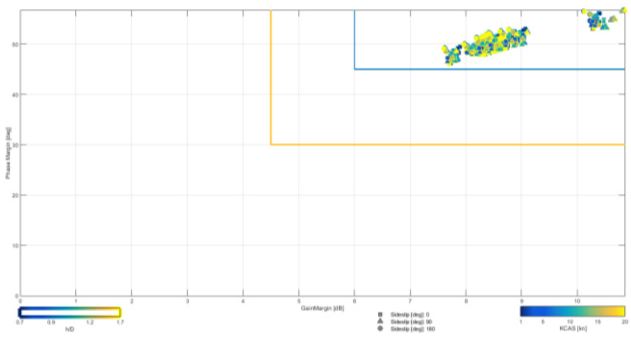

Figure 34: Canonical SISO Stability Margins of perturbed models WCG1, Roll Rate loop open (x-axis GM, y-axis PM)

6.3. Worst case conditions selection

Worst conditions from closed-loop dynamic stability analysis, corresponding to worst aperiodic and periodic modes (highest eigenvalue real part) for each weight and balance configuration, was selected from the results obtained on nominal and perturbed models along all trim conditions. While in terms of robustness, one worst case for each W/CG was extracted, namely the lowest values of disk-based margins along nominal and perturbed models and all the trims. The results are listed in Table 4, indicating for each worst case the trim parameters, the SCAS channel (LON, LAT, DIR) where the minimum margins were found and the perturbed model ID (model 0 is the nominal).

Worst	WCG	AoS [deg]	V [kts]	h/D	SCAS ch.	Model ID
periodic	1	90	10	0.9	-	19
aperiodic	1	180	10	0.9	-	26
margins	1	90	20	1.2	LON	20
periodic	2	90	10	0.9	-	19
aperiodic	2	180	10	0.9	-	26
margins	2	90	20	1.7	LON	1
periodic	3	90	10	0.9	-	19
aperiodic	3	180	10	0.9	-	26
margins	3	90	20	0.7	LON	18

Table 4: Worst conditions selection

6.4. Stability analysis on worst cases applying actuators uncertainties

The impact of actuation performance spread on closed-loop A/C dynamic stability was analyzed by combining the worst case conditions found considering only the bare A/C uncertainties in Table 4, with the swashplate actuators perturbation in Table 2. In Figure 35 are showed only the closed-loop eigenvalues non-compliant respect to TR.181(c) on the Gauss plane, along the aforementioned conditions in terms of trim, perturbed bare A/C model and actuators perturbation. The low-frequency deviations from TR.181(c) have been compared also against less conservative MIL-H-8501A VFR boundaries and ADS-33 Level 2. The bigger marker indicates for reference the non-compliant eigenvalues of the worst case with nominal swashplate actuator dynamics. The picture is slightly worsened with perturbed swashplate actuation models, bringing some eigenvalues marginally outside the ADS-33 limit (5sec. time to double), albeit still reasonably compliant with above specifications. In Figure 36 the histogram representation allows to appreciate the non-compliance occurrences percentage distribution in terms of mode shape: only longitudinal modes are involved as already found without actuators perturbation.

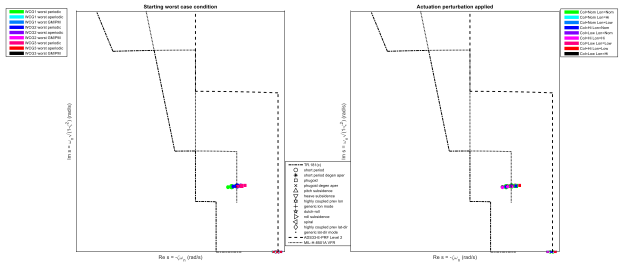

Figure 35: Root-locus worst case closed-loop models with actuation perturbation, requirements deviations (left: sensitivity to worst conditions, right: sensitivity to actuation models, bigger marker: nominal actuation). Different requirements comparison

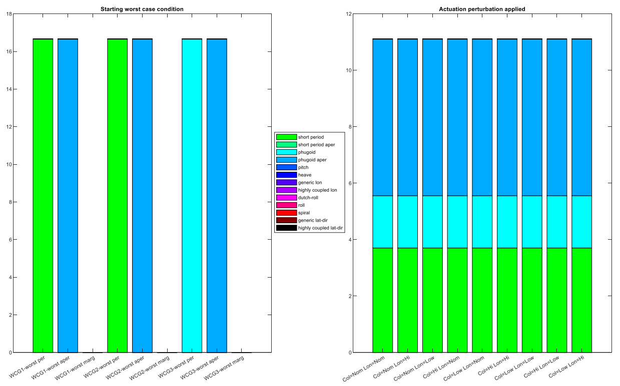

Figure 36: Worst case closed-loop models with actuation perturbation, dynamic stability requirement deviation occurrences percentage respect to mode shape (left: sensitivity to worst conditions, right: sensitivity to actuation models)

Moreover, the Figure 36 left subplot shows that the non-compliances are exactly equidistributed over the worst dynamic stability cases (whatever is the WCG), without occurrences for the robustness worst conditions: when the starting worst case with nominal actuation is non-compliant in terms of dynamic stability, it remains eigenvalues placement type non-compliant including actuation perturbation. While from the right subplot the non-compliances are exactly equidistributed over the swashplate actuator perturbation: there is no one combination worse than the others. In Figure 37 the non-compliance occurrences are grouped by unstable mode time to double ranges in abscissa, while the bar colors indicates distribution in terms of worst condition and actuator perturbation: as the results without actuators uncertainties the majority of on-compliances have time to double higher than 9sec and between 5 and 9sec, but the actuators perturbation implies some cases with T2 slightly below the ADS-33 Level3 5sec. limit.

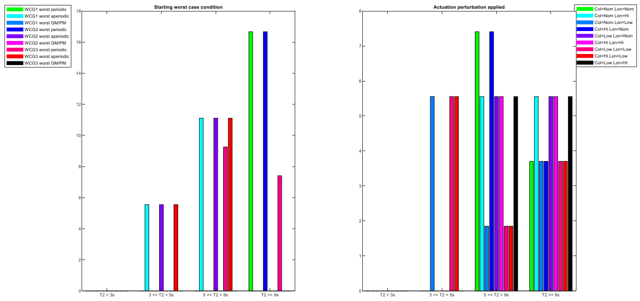

Figure 37: Worst case closed-loop models with actuation perturbation, dynamic stability requirement deviation occurrences percentage respect to mode time to double (left: sensitivity to worst conditions, right: sensitivity to actuation models)

6.5. Robust stability analysis on worst cases applying actuators uncertainties

The influence of actuators uncertainties on the robust stability is discussed hereafter. In Figure 38 the histogram representation shows how the total gain and phase disk-based margins non-compliance occurrences percentage are distributed along the SCAS channels: the majority are on the longitudinal (pitch rate sensor opening), then lateral and only few cases on the directional one. The left subplot shows that the non-compliances occur only on worst margins cases (whatever is the WCG), without occurrences on the dynamic stability worst conditions (conversely to what observed in Figure 36 for the dynamic stability results): when the starting worst case with nominal actuation is non-compliant in terms of robust stability, it remains robustness non-compliant including actuation perturbation. While from the right subplot the non-compliances occur on specific actuators perturbation combinations. For sake of brevity the disk-based gain and phase margins as a function of the frequency are showed only for roll rate sensor opening in Figure 39 and Figure 40, with sensitivity respect to worst conditions and actuators uncertainties combinations. The bigger marker represents as reference the stability margins without actuators perturbation: the added uncertainties do not always imply a worsening of the margins. Non-compliances detected respect to SAE requirements arise only at low frequency (below 0.06Hz), and it is the same also for the other SCAS channels. In Figure 41 phase margin non-compliances percentage occurrences distribution on worst conditions and actuators uncertainties is presented, grouped in three phase margin ranges, from zero to the required SAE value. While Figure 42 shows a similar representation but with the corresponding grouping in frequency for the phase margin non-compliances: from 0 to the SAE threshold at 0.06Hz, from 0.06 to 1Hz, and from 1Hz to FAM frequency.

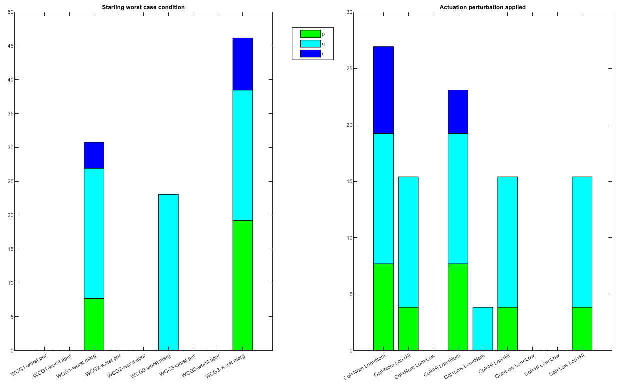

Figure 38: Disk Margin of worst models with actuation perturbation, requirement deviation occurrences percentage, sensitivity respect axis, loop broken at sensors interface (left: sensitivity to worst conditions, right: sensitivity to actuation models)

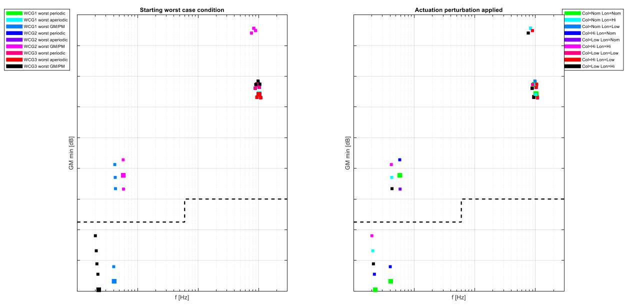

Figure 39: Disk Gain Margin worst models with actuation perturbation, loop open on roll rate (left: sensitivity to worst conditions, right: sensitivity to actuation models, bigger marker: nominal actuation)

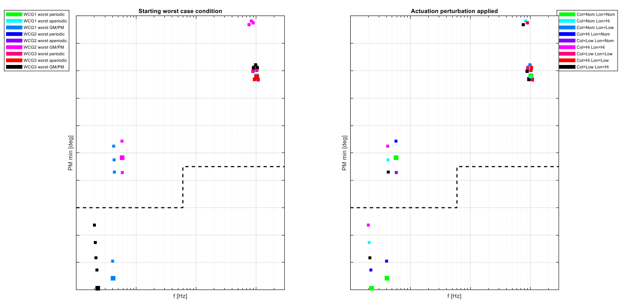

Figure 40: Disk Phase Margin worst models with actuation perturbation, loop open on roll rate (left: sensitivity to worst conditions, right: sensitivity to actuation models, bigger marker: nominal actuation)

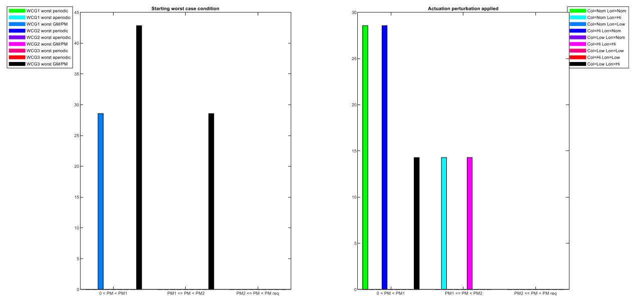

Figure 41: Disk Phase Margin of worst models with actuation perturbation, loop open on roll rate, requirement deviation occurrences percentage, sensitivity respect phase margin ranges below requirement limit

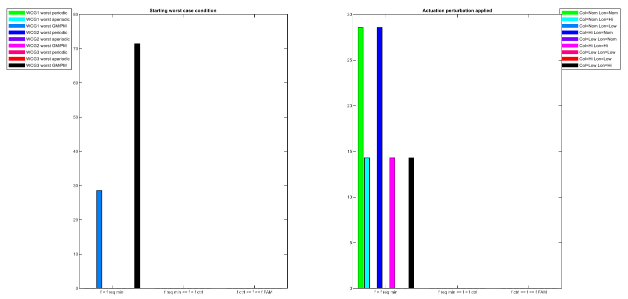

Figure 42: Disk Phase Margin of worst models with actuation perturbation, loop open on roll rate, requirement deviation occurrences percentage, sensitivity respect frequency ranges

7. CONCLUSIONS

The paper described the entire numerical process to evaluate the robust stability of a tiltrotor. First, it was developed a physics-based approach to build a family of uncertainty bare aircraft flight dynamics models, perturbing only a limited number of aeromechanics parameters, according to the estimated level of uncertainty from the nominal value, instead of the traditional Monte Carlo approach to parametric model perturbation, which implies a huge number of trials. Then the robustness of designed aircraft FCS control laws to these uncertainties was assessed adopting a disk-based stability margins approach rather than the classical one. It guarantees a more complete (because frequency-wise) and reliable evaluation of stability robustness, and moreover consents to potentially deal with unstable dynamics, when in canonical sense the margins are null by definition. Because of a sort of dichotomy between the dynamic stability requirements of TR.181 for tiltrotor in VTOL/Conversion mode, which allows low frequency unstable modes in closed-loop, and robustness requirements of SAE-AS-94900 requiring positive stability margins defined in the canonical sense, the verification of robust stability requirement should be done also in presence of closed-loop unstable modes. Although the processing of disk-based stability margins is not well posed at frequencies corresponding to unstable modes, it was specifically developed a novel approach in the choice of the lower bound of computation frequency range along which the disk margins are evaluated, based on closed-loop system eigenvalues placement: a disk computing exclusion zone is defined to avoid the stability margins drop bias due to unstable modes presence and therefore extract a meaningful measure of the robustness in the frequency range of interest for the control, also when the closed-loop aircraft dynamics is unstable.

The proposed methodology has been applied to NGCTR-TD tiltrotor in helicopter configuration, in hover and near hover IGE conditions, to assess the closed-loop dynamic stability of a new Fly-By-Wire rotorcraft for which no experimental flight data exist yet, as part of the clearance process for the initial phase of flight testing activities, verifying the control laws robustness to the modelling uncertainties in the linear (frequency) domain.

- Accordingly to the obtained analysis results, dynamic stability requirements given by TR.181(c) are almost fully met by the NGCTR-TD, with minor deviations at very low frequency, but compliant with both MIL-H-8501A VFR guidelines and 5 seconds time-to-double requirement expressed by ADS-33. These deviations are considered acceptable from a practical standpoint, especially considering the degraded CLAWs configuration (providing basic rate stabilization only) and the IGE flight conditions, characterizing the first phase of the aircraft flight test campaign. The worst dynamic stability cases predicted by the conducted analysis in the linear domain will be further analyzed through pilot-in-the-loop assessments at engineering simulator.
- While in terms of robustness, the SAE-AS-9490 requirements are fundamentally met by the NGCTR-TD, especially at frequencies of interest for CLAWs loop closures: the minor deviations encountered around 1Hz were considered acceptable considering the inherent conservatism associated with the adopted disk margin approach and recalling that SAE limits are defined in terms of canonical margins. While the detected insufficient stability margins below 0.06Hz were not considered of any practical concern because the disk margin processing is affected by the nearby unstable modes, which are considered acceptable based on the dynamics stability requirements. In other words, these robustness non-compliances at very low frequency derive from poorly harmonized dynamic and robust stability requirements.

The planned further activities on the subject matter include:

- validation and refinement of the nominal bare A/C flight dynamics model and the related perturbation methodology, by means of a dedicated identification flight test campaign of the NGCTR-TD
- reiteration of the whole described numerical process to evaluate closed-loop dynamic stability and its robustness to clear each envisaged incremental step of the NGCTR-TD flight envelope expansion test campaign
- evaluation of include explicitly in control laws synthesis optimization process at least the worst case perturbed models, enforcing a robust design but keeping computational burden to reasonable levels

Authors contact:

Fabio Riccardi:

fabio.riccardi@leonardo.com

Luca Viganò:

luca.vigano01@leonardo.com

Francesco Marzagalli:

francesco.marzagalli@leonardo.com

8. ACKNOWLEDGMENTS

This work was performed as part of the project NGCTR-TD and has received funding from the Clean Sky 2 Joint Undertaking (JU). The JU receives support from the European Union’s Horizon 2020 research and innovation programme and the Clean Sky 2 JU members other than the Union.

This paper reflects only the author’s view; the JU is not responsible for any use made of the information contained herein.

9. REFERENCES

1. S. W. Ferguson, "*Development and validation of a simulation for a generic tilt-rotor aircraft*", NASA CR-166537.

2. S. W. Ferguson, "*A mathematical model for real-time flight simulation of a generic tilt-rotor aircraft*", NASA CR-166536.

3. F. Porcacchia, F. Riccardi, A. Mancini, M. Pecoraro, A. Ragazzi, L. Viganò, "*Assessment of Numerical Approaches for Modelling Tilt-Rotor Ground Effect stability in Hover and Near Hover Conditions*", Vertical Flight Society's 79th Annual Forum & Technology Display Proceedings, West Palm Beach, FL, USA, May 16-18, 2023

4. Zhou, K., Doyle, J.C., *Essentials of Robust Control,* Prentice Hall, 1998

5. S. Panza, M. Lovera, M. Sato, K. Muraoka, "*Structured μ-Synthesis of Robust Attitude Control Laws for Quad-Tilt-Wing Unmanned Aerial Vehicle*", Journal of Guidance, Control, and Dynamics, Vol.43, No.12, 2020

6. Apkarian, P. and Noll, D., *"Non-smooth H-infinity Synthesis"*, IEEE Transactions on Automatic Control, Vol. 51, No. 1, 2006

7. Tischler, M. B., Berger, T., Ivler, C. M., Mansur, M. H., Cheung, K. K., and Soong, J. Y., *"Practical Methods for Aircraft and Rotorcraft Flight Control Design: An Optimization-Based Approach"*, AIAA, 2017, Reston, VA.

8. Berger, T., *"Handling Qualities Requirements and Control Design for High-Speed Rotorcraft"*, Special Report FCDD-AMV-20-01, February 2020

9. http://www.flightlab.com

10. L. Viganò, C. Punzi, F. Riccardi, F. Porcacchia, *"Investigation of Coupled Torsional Stability Analysis Methodology for Tiltrotor: the Helicopter Mode case"*, Vertical Flight Society's 80th Annual Forum & Technology Display Proceedings, Montréal, Quebéc, Canada, May 7-9, 2024

11. T. Femi and S.J. Mija, *"Modelling of Hovering Helicopter and its Stability analysis using Participation Factor"*, IFAC PapersOnLine 51-1 (2018) 504-511

12. Blight, J.D., R.L. Dailey, and D. Gangsaas, *"Practical Control Law Design for Aircraft Using Multivariable Techniques"*, International Journal of Control. Vol. 59, No. 1, 1994, pp. 93–137

13. Seiler, P., Packard, A., and Gahinet P., *"An Introduction to Disk Margins"*. [Lecture Notes]. IEEE Control Systems Magazine 40, no. 5 (October 2020): 78–95

14. SAE-AS-94900 rev.A, *"Aerospace Standard - General Specification for Design, Installation and Test of Piloted Military Aircraft Flight Vehicle Management Systems – Flight Control Function"*, August 2018

15. http://www.rocs-project.org

16. Chengjian He, *"Development and application of a generalized dynamic wake theory for lifting rotors"*, Georgia Institute of Technology July, 1989

17. Cantoni, M. and Vinnicombe, G., *"Quantifying uncertainty and robust performance using the ν-gap metric"*, AIAA Guidance, Navigation and Control Conference, Portland, USA, pages 1624–1630, 1999.

18. MIL-H-8501 issue A, *"Military Specification – General Requirement for Helicopter Flying and Ground Handling Qualities"*, September 1961

19. ADS-33E-PRF, *"Aeronautical Design Standard - Performance Specification - Handling Qualities Requirements for Military Rotorcraft"*, March 2000

20. Weissinger, J., *"The lift distribution of swept-back wings"*, NACA TM 1120